Toward Temporal Fiber

Matthew Ozon, Marc Robini, Pierre Croisille, Carole Frindel, Yue-Min Zhu

CREATIS CNRS UMR 5220, INSERM U1044, Universite Lyon 1, INSA Lyon, Lyon, France

Abstract

One of the next challenges of DTI in cardiac domain is to assess moving fibers. An important bottleneck is the acquisition time due to the angular resolution required to extract accurate myocardial fibers. Therefore, the creation of a method able to extract reliable fibers from low angular resolution is a key point to accelerate DTI acquisition, consequently a considerable step toward temporal fibers. In this study we introduce a graph-based method for fiber tracking and evaluate its performances.

1. Introduction

The fibrous architecture of human heart is of upmost importance in myocardium mechanics and for our understanding of malformations and structural diseases. To date, research on heart fiber conformation is mainly based on histology [1] or diffusion tensor imaging (DTI) [2]. However, only DTI can be used for in-vivo investigations, but, current fiber tracking algorithms often fail if the number of gradient directions used for the acquisition is too low. As a consequence, assessing the fiber structure of in-vivo heart is often not reliable. Hence, a relevant improvement is to create a method that is able to accurately extract fibers under those conditions. In addition to increase the quality of the tractogram, it could help relaxing constraints on in-vivo acquisition.

The aim of our study is to find the lower bound of number of gradient directions required to extract good fibers. For this purpose, we try a global approach based on graph representation similarly to the study conducted in [2]. In this paper, we introduce the mathematical framework for the formulation of the tracking problem. Then, we present the results obtained for the characterization of our method.

2. Graph-based representation

We describe the data with graphs in which the set of vertices $\mathcal{V}$ is the set of spacial points inside a volume of interest and are associated to a Diffusion Tensor (DT). The set of edges $\mathcal{E}$ binds neighbor vertices. All edges are binary weighted so that neighbors are always linked but they can be either connected (weight 1) or not (weight 0). The neighborhood $\mathcal{N}_v$ of a vertex v if defined by all the vertices that are included in a ball centerd on v and of radius $R \in \mathbb{R}^{+*}$. We will denote the graph $\mathcal{G} = (\mathcal{V}, \mathcal{E})$ and for each edge $e \in \mathcal{E}$ we note $\omega_e \in \{0, 1\}$ the edge state and Ω the set of all edge states, namely graph configuration. $\mathcal{G}_{\Omega} = (\mathcal{V}, \mathcal{E}, \Omega)$ stands for the graph $\mathcal{G}$ in the configuration Ω.

We define a fiber as a non-cyclic sequence ϕ of vertices which define the control points of the underlying continuous fiber, $\phi = (v_{i_k})_{i_k}$ where $(i_k)_{k \in \mathbb{N}}$ is a sequence of indices. Edges can be considered as the smallest possible fibers.

The point in using graph representation is to easily model interactions between neighbors, which is a key point of our model, as recently pointed out in [3]. Moreover, graphs have interesting properties that will be used for the optimization problem.

3. Fiber tracking: formulation

The eigenvector of the main eigenvalue of DT is highly correlated with the main diffusion direction [1]. We define a vector field $\overrightarrow{F}$ as the field of main unit eigenvectors weighted by the fractional anisotropy (FA). Hence, the definition of an objective cost due to the linear path, through the field, $G \subset \mathbb{R}^3$, of finite length L:

$$A_{\mathrm{G}} = \frac{-1}{L} \int_G \left| \overrightarrow{F}(x) \, \mathrm{d}\overrightarrow{x} \right|$$

A_{G} is small when G fits the vector field, on the contrary, if the element is orthogonal to the field, it does not contribute and A_{G} is larger. Beside, the FA weighting ensures only reliable data affect the integral. To not foster the largest elements, but the best matches, we normalize by the length.

Let consider a vertex $v \in \mathcal{V}$ and two edges e_1 and e_2 in $\mathcal{N}_v$. A small fiber supported by e_1 and e_2, at v, is denoted $\phi_{\{e_1, e_2\}} \subset \mathbb{R}^3$. We consider that edges interact with their neighbors separately and uniformly, which is translated in the following formula:

$$U_s(v) = \frac{1}{Z_v} \sum_{\{e_1, e_2\} \in \mathcal{N}_v} \omega_{e_1} \omega_{e_2} A_{\phi_{\{e_1, e_2\}}}$$

where the binary degree Z_v is the number of connected pairs if at least one pair exists and 1 otherwise.

The interaction model based on the binary clics is twofold. First, the integral is calculated over an interpolation curve of the three points forming the edge pair. Second, edges interact with one other edge at once in the product $\omega_{e_1}\omega_{e_2}$. Those interactions slightly modify the behavior of the energy in comparison to a unary interaction model.

However, the problem remains ill-posed where the DT are not prolate. Indeed, a non-prolate DT means that several diffusion directions are possible, thus the problem must be regularized. We introduce two terms that stems from our prior knowledge on cardiac fibers: U_c for the smoothness assumption and U_i to avoid the crossing configurations. The global energy is the sum of the three contributions over the graph:

$$U(\mathcal{G}_\Omega) = \sum_{v \in \mathcal{V}} U_s(v) + \alpha U_i(v) + \beta U_c(v)$$

where α and β are topological balance term in $\mathbb{R}^+$ and modify the energy landscape, therefore, the tractogram.

4. Simulated annealing

Simulated Annealing (SA) is a generic method for combinatorial optimization that is quite popular because of its ease of implementation and its global convergence properties. The key feature of SA is that it allows uphill moves (that is, moves that increase the value of the energy function) in order to escape local minima. By analogy with the physical process of annealing in solids, uphill moves are accepted with a certain probability controlled by a temperature parameter that decreases monotonically to zero. The following section gives a formal description of SA, followed by the main convergence results.

Let U be a real valued function to be minimized on a general but finite state space Ω. An SA algorithm with cost function U is a discrete time, non-homogeneous Markov chain $(\Gamma^{(n)})_{n \geq 0}$ whose transitions are guided by a communication mechanism q and controlled by a cooling sequence $(T_n)_{n \geq 0}$. The communication mechanism gives the probabilities of the possible moves for generating a candidate solution from the current solution, and the cooling sequence decreases to zero. Formally, q is a map from Ω^2 to $[0,1]$ that has the following properties:

1 q is a Markov matrix: $\forall \omega \in \Omega, \sum_{\rho \in \Omega} q(\rho,\omega) = 1$
2 q is symmetric: $\forall (\rho, \omega) \in \Omega^2, q(\rho,\omega) = q(\omega,\rho)$
3 q is irreducible: $\forall (\rho, \omega) \in \Omega^2, \exists$ a path $(\gamma^{(n)})_{0 \leq n \leq K}$ such that $\gamma^{(0)} = \rho, \gamma^{(0)} = \omega$, and $q(\gamma^{(k)}, \gamma^{(k+1)}) > 0$ for all $k \in [\![0, K-1]\!]$.

Property 2 means that the probability to propose a move from ρ to ω is the same as to propose a move from ω to ρ, and property 3 means that any state can be reach from any other state in a finite number of moves. The transition of

$(\Gamma^{(n)})_{n \geq 0}$ are given by:

$$P\left(\Gamma^{(n)} | \Gamma^{(n-1)}\right) = P_{T_n}(\rho,\omega)$$

where P_T is the Markov matrix on Ω defined by:

$$P_T(\rho,\omega) = \begin{cases} q(\rho,\omega) \text{ if } U(\omega) < U(\rho) \text{ and } \rho \neq \omega \\ q(\rho,\omega)\, e^{-\frac{U(\omega)-U(\rho)}{T}} \text{ otherwise} \end{cases}$$

Putting it simply, downhill moves are unconditionally accepted, whereas an uphill move from ρ to ω is accepted wit the probability $e^{-\frac{U(\omega)-U(\rho)}{T}}$. In practice, a finite-time realization $(\gamma^{(n)})_{0 \leq n \leq N}$ of $(\Gamma^{(n)})_n$ is generated as described in Algorithm1.

Pick an initial state $\omega^{(0)} \in \Omega$;
for *n=1 to N* **do**

> draw a state ρ from the distribution $q(\omega^{(n-1)}, \bullet)$;
> set $\omega^{(n)} \leftarrow \omega^{(n-1)}$;
> set $\Delta U \leftarrow U(\rho) - U(\omega^{(n-1)})$;

if $\Delta U \leq 0$ **then**

> set $\omega^{(n)} \leftarrow \rho$;

else

> set $\omega^{(n)} \leftarrow \rho$ with probability $e^{-\frac{\Delta U}{T_n}}$;

end
end

Algorithm 1: SA algorithm pseudo-code

As the temperature T_n goes to zero, the distribution of $\Gamma^{(n)}$ concentrates on the global minima of U, and SA does indeed converge to a global minimum it $T_n \propto \frac{1}{\ln(n+1)}$ [4]. However, logarithmic cooling yields to extremely slow convergence and most successful application of SA use exponential schedules. The theoretical justification of exponential cooling is given in [5], where it is shown that the convergence speed exponent of SA has an upper limit α_{opt} and that it is possible to construct a family $\left\{ (T_n)_{1 \leq n \leq N} ; N \geq 1 \right\}$ of finite cooling sequence of the form $T_n = T_0 e^{-\lambda n}$, where $\lambda \in]0, \infty[$ depends on N, such that:

$$\ln\left(P\left(U\left(\Gamma^{(N)}\right) > \inf_{\omega \in \Omega} U(\omega) \right) \right) \sim \ln\left(N^{-\alpha_{\text{opt}}} \right)$$

These results are not well known, but yet they constitute the most significant advance in SA theory beyond the asymptotic properties established in [4]. They imply in particular that for any $\alpha \in]0, \alpha_{\text{opt}}[$ there is a family $\left\{ (T_n)_{1 \leq n \leq N} ; N \geq 1 \right\}$ of finite exponential cooling sequence such that:

$$P\left(U\left(\Gamma^{(N)}\right) > \inf_{\omega \in \Omega} U(\omega) \right) \sim N^{-\alpha}$$

for N large enough. In other words, exponential cooling makes it possible for SA to have a convergence speed exponent arbitrarily close to the best exponent over all possible cooling sequences. More elaborated developments in SA theory can be found in [6].

5. Measure

In this study we try to quantitatively characterize the behavior of our algorithm. Consequently, we need to define quantities that are able to describe fibers with scalars. We define two quantities which are related and that estimate the angle deviation and the similarity between two fiber sets. The measures that we introduce are strongly related to the measures introduce in the "fiber cup" contest described in [7]. However, those are only available for fully known data, such as synthetic data.

In order to assess the similarity between two fibers, the first step is to define a distance. Let consider an extracted fiber ϕ and its parameterized approximation $\varphi \in \mathcal{C}^\infty([0,1],\mathbb{R})$. Let also assume that a parameterization ζ_ξ of the theoretical GT fiber is known for whole volume and controlled by a finite set of parameters ξ.

The distance from the extracted fiber to the closest theoretical one is given by:

$$m(\phi) = \min_{\mathbf{t},\xi} \frac{1}{N} \sum_{i=1}^{N} \| \varphi(t_i) - \zeta_\xi(t_i) \|_2^2$$

where $\mathbf{t} = \{t_i \in [0,1] \mid i \in [\![1, N]\!]\}$. Using the smoothness assumption, we can define the tangent to the curves at each point as the first derivative. Hence, the definition of a mean deviation between the two fibers comes forward, and is named the mean deviation angle:

$$\gamma(\phi_s, \xi_0, \mathbf{t}_0) = \frac{1}{N} \sum_{i=1}^{N} \left(\zeta'_{\xi_0}(t_{0_i}) , \varphi'(t_{0_i}) \right)$$

where $\mathbf{t}_0$ and ξ_0 denote the sets of arguments that define $m(\phi)$. Both previous quantities let us create a similarity measure $\tilde{\Xi}$ for a set Φ of K fibers, and:

$$\tilde{\Xi}(\Phi) = \frac{1}{K} \sum_{\phi \in \Phi} \frac{m(\phi) \sin(\gamma(\phi, \xi_0, \mathbf{t}_0))}{L_\phi}$$

where L_ϕ is the physical length of ϕ.

6. Results

Data: For our experiments we use two kind of data: simulated and real. The synthetics data are involved in the characterization process because we perfectly now their structures which tend to mimic the left ventricle. They are in a hollow cylinder form, which main axis corresponds to

the short axis, and the helix angle is constant (for practical reason). The real data were acquired on an ex-vivo human heart with a Siemens Avanto 1.5T MR Scanner. The Diffusion Weighted Images (DWI) were obtained using an echo planar imaging pulse sequence with the following parameters: image reconstructed to 128×128 matrix, isotropic voxel size $2 \times 2 \times 2 \, \mathrm{mm}^3$, 54 axial contiguous slices. The DTI acquisition protocol was characterized by 12 encoding gradient directions and 6 repetitions per direction. The repetition time was fixed to 8600ms and the b-value to $1000 \, \mathrm{s.mm}^{-2}$.

Experiments: We study the behavior of our algorithm from two view points: the quality and the quantity of DWI.

In order to characterize our algorithm (U15) to the quality of DWI, we study extracted fibers from a synthetic data set with different noise levels, in a range from the noiseless data to a SNR of 1 (information from data is as much important as the noise). We corrupted the data by adding a rician noise on the DWI. For each noise level, three fiber tracking methods were run, ours, another graph-based method referred to as U1 [2] and a streamline (STRK4) described in [8]. We measure two indices for each fiber set: the angular deviation and the similarity measure. The results are depicted in figure 1. We note that U15 shows a
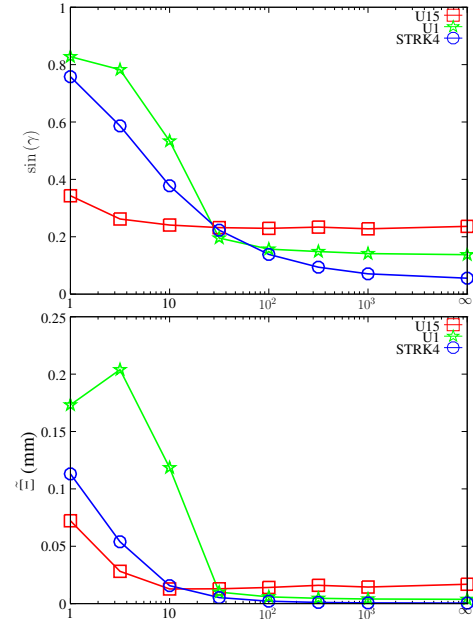

Figure 1. Characterization of our method to the noise in DWI using angular deviation (top) and similarity (bottom) for eight SNR in synthetic data. The three methods, U15, U1 and STRK4, are respectively represented by the red curves with square marker, the green curves with star-shape makers and the blue curves with circles.

systematic angle bias, almost constant over the whole SNR range, contrary to U1 and STRK4 which seem to com-

pletely lose their angular accuracy with the noise level. On the similarity graph, we can see that for high SNR (≥ 100) U15 has a higher score than U1 and STRK4, and for low SNR (≤ 10) the trend is inverted. This observation means that U1 and STRK4 extract good fibers in high quality images, but fail with poor quality acquisition. On the contrary, U15 do not show very precise results at high SNR, yet the fibers are usable for visual expertise. However, U15 outperforms at low SNR which is most likely to be a consequence of the addition of prior knowledge in the model.

To better evaluate the performances of a fiber tracking method in DTI context, it is relevant to show the behavior with the number of DWI. Indeed, less DWI means a lower angular resolution and precision in the DT, which could decrease the quality of extracted fibers, but it would also mean faster acquisitions.

To emphasis the robustness of U15 to low angular resolution, we extracted fibers on the human heart data set using two conditions, one with all the data (12 directions, 6 repetitions) and another with only 6 directions not averaged. We measured the helix angle of the left ventricle wall in a middle slice Fig 2. We notice on Fig 2 that the
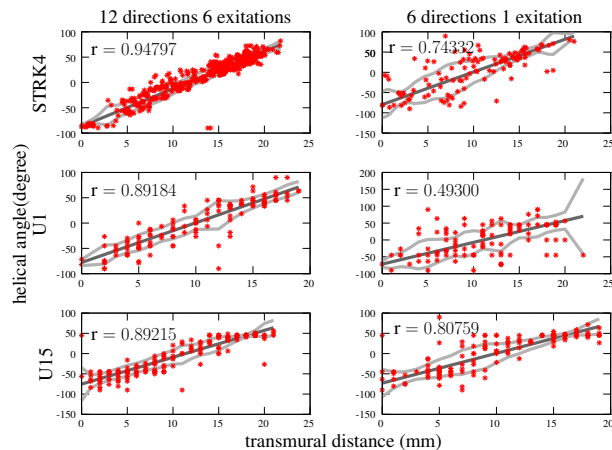

Figure 2. Helical angle on real heart. Two angular resolutions are involved: 12 gradient directions with 6 repetitions (left column) and 6 directions with no repetition (right column). For the three methods, STRK4, U1 and U15 we show the helical angle according to the transmural distance from the epicardium to the endocardium. The measured angles in a transmural sample are plotted as red asterisk, the thick gray line is fitted in the population and the light gray lines are the one-standard deviation envelopes.

correlation between helix angle and wall depth is similar to the results found in [9]. We also observe that the correlation coefficients of distribution of the helix angle with the wall depth is the highest for the streamline at full angular resolution, but for the low angular resolution, the best coefficient is for our method. We also note that the decrease in r is lower for U15 than STRK4, which indicates that an-

gular accuracy is not lost with lower resolution, but it can be retrieved with more complex model than a streamline, even at precision cost.

7.   Conclusion

This study brings out the possibility to extract good fibers in low angular resolution situation merely by improving the interaction model of the function describing the tractography problem without using a too complex model of the physical underlying diffusion process. Therefore, one must focus on how to best describe the tractography problem with mathematical tool so that we can mine most of the hidden information in low angular resolution DWI. Those efforts could lead to possible relaxations on the constraints of acquisition, so that it can be sped up.

References

[1] Scollan D, Holmes A, Winslow R, Forder J. Histological validation of myocardial microstructure obtained from diffusion tensor magnetic resonance imaging. American Journal of Physiology Heart and Circulatory Physiology 1998; 275(6):H2308–H2318.

[2] Frindel C, Robini M, Schaerer J, Croisille P, Zhu Y. A graph-based approach for automatic cardiac tractography. Magnetic Resonance in Medicine 2010;64(4):1215–1229.

[3] Mangin JF, Fillard P, Cointepas Y, Bihan DL, Frouin V, Poupon C. Towards global tractography. NeuroImage 2013;.

[4] Hajek B. Cooling schedules for optimal annealing. Mathematics of operations research 1988;13(2):311–329.

[5] Catoni O. Rough large deviation estimates for simulated annealing: Application to exponential schedules. The Annals of Probability 1992;1109–1146.

[6] Robini MC. Theoretically grounded acceleration techniques for simulated annealing. In Handbook of Optimization. Springer, 2013; 311–335.

[7] Fillard P, Descoteaux M, Goh A, Gouttard S, Jeurissen B, Malcolm J, Ramirez-Manzanares A, Reisert M, Sakaie K, Tensaouti F, Yo T, Mangin J, Poupon C. Quantitative evaluation of 10 tractography algorithms on a realistic diffusion mr phantom. Neuroimage 2011;56(1):220–234.

[8] Basser P, Pajevic S, Pierpaoli C, Duda J, Aldroubi A. In vivo fiber tractography using dt-mri data. Magnetic resonance in medicine 2000;44(4):625–632.

[9] Lombaert H, Peyrat J, Croisille P, Rapacchi S, Fanton L, Cheriet F, Clarysse P, Magnin I, Delingette H, Ayache N. Human atlas of the cardiac fiber architecture: Study on a healthy population. Medical Imaging IEEE Transactions on 2012; 31(7):1436–1447.

Address for correspondence:

Ozon Matthew
CREATIS - INSA LYON , Bâtiment Blaise Pascal, 7 Avenue Jean Capelle, 69621 Villeurbanne Cedex
ozon@creatis.insa-lyon.fr